Five transiting exoplanets observed and analyzed using the MDM 1.3 meter telescope.

Ethan Henley[1], James Gong[1], Cameron Nuñez[1], and Gabrielle Suissa[1]

Observational Astronomy Class, Columbia University

May 11, 2018

ABSTRACT

Over three different nights in March and April 2018, we took a series of observations with the McGraw-Hill 1.3 meter telescope at the MDM observatory. Each observation targeted a specific star known to host an exoplanet with a transit predicted for the time of observation. Each observation was timed to measure either the duration or half the duration of the predicted transit. Each observation consisted of regular imaging of a target star and the surrounding sky. Photometric analysis of each series of images yielded light curves of varying clarity for each star. Of the five observations, two produced clear transits: TReS-3 and HAT-P-12. Depth measured of those stars' light curves suggested planetary radii of $1.268^{+0.023}_{-0.034} R_J$ for TReS-3b and $1.336^{+0.031}_{-0.036} R_J$ for HAT-P-12. In conjunction with previous measurements of these stars, we determined that TReS-3 and HAT-P-12b are each gaseous planets.

Key words. Observational; Planetary Detection; David Schiminovich; Jose Manuel Zorrilla

1. Introduction

One major application of astronomical photometry is time series photometry, from which we can discover exoplanets using the transit method. In the light curves of a star, transiting planets can be detected by dips in brightness levels. Light curves of stars are graphs that show the star's brightness over a period of time. The transit method has been used to discover a host of exoplanets over the last decade, especially as space-based telescopes such as Kepler can detect smaller dips in light curves caused by transiting planets. Exoplanet discoveries using the transit method now greatly outnumber other methods such as radial velocity and gravitational microlensing. Detecting exoplanets, especially those that orbit in a star's habitable zone, are an important field of scientific discovery. It has also helped inform us of the frequency of exoplanets around stars in our galaxy, and helped inform astrobiological estimates. Though smaller than the telescopes used in these projects, the McGraw-Hill telescope is powerful enough to analyze and inspect already-confirmed exoplanets.

We were presented the opportunity to collect our own time series photometry using the 1.3m telescope at the MDM Observatory in Arizona, from which we could analyze collected data for exoplanet transits. We observed on location the morning of March 13, 2018. We also conducted two nights of remote observation on April 3, 2018 and April 4, 2018. Our project serves as a demonstration of ground-based observation for exoplanet transit detection.

Our exoplanet targets were previously discovered by surveys conducted by ground-based telescopes designed to search for exoplanets. The HAT (Hungarian Automated Telescope) survey is maintained by the Harvard-Smithsonian Center for Astrophysics, and HAT-South is an extension of the original network consisting of three telescopes in the Southern Hemisphere. The XO Project makes use of the XO Telescope, located on the summit of Haleakala in Hawaii. The Trans-Atlantic Exoplanet Survey (TReS) uses three 4-inch telescopes located at Lowell Observatory, Palomar Observatory, and the Canary Islands.

2. Selecting Targets

In order to select appropriate transiting exoplanet targets, we considered several factors. We utilized the Exoplanet Transit Database (http://var2.astro.cz/ETD/) to find exoplanets that we could observe during our nights at MDM Observatory. We first ensured that the stars observed had an apparent magnitude no less than 10, as a very bright star would be saturated and unfit for long exposures. We also checked that our targets were not too near the moon in order to reduce additional contributions. We then had to consider the star's altitude. It is imperative to select a target not too low on the horizon. Not only would a low-altitude star potentially sink below the horizon over the course of the night, but it would also suffer from an increase in air mass because a lower visual path cuts through more of the atmosphere. The high air mass of a low-altitude star thus obscures the visibility of the star. In addition, many telescopes have a minimum angle above the horizon, beneath which they can be damaged. For the MDM Observatory in particular, the cut off angle renders the telescope incapable of rotating lower than about 20 degrees, affecting our choices of transits to select.

In general, there are also many factors that determine whether a planet of a certain size can be detected with a particular telescope, including the duration of the transit, stellar variability, the size of star, and the brightness of the star. Due to MDM being a ground-based observatory, and our access to a mirror of 1.3 meters in diameter, we expect to only detect large planets - likely hot Jupiters - because they are large enough to block out significant amounts of light, and close enough to the star so that their size is prominent. It is this observational bias that constrains our selection of exoplanets for this project.

For this project, we selected the target star HATS-18, a G star of apparent magnitude 14.0, to observe during the morning

of March 14, 2018 at MDM. For our remote observing nights (located at the lovely office of Professor David Schiminovich, provided by Columbia University's special partnership with MDM), we observed TrES-3, a G star with an apparent magnitude of 12.4, and XO-2, a K star with an apparent magnitude of 11.18 on the morning of April 4. Finally, on the morning of April 5, we remotely observed HAT-P-12 and HAT-P-26, two K stars of apparent magnitudes of 11.74 and 12.84, respectively.

All in all, we had five promising exoplanet targets, all which matched the criteria described above.

3. Collecting Data

A large component of this project was familiarizing ourselves with the process of using large-scale telescopes like the 1.3 meter one at the MDM Observatory. Generally, if one uses the telescope correctly, one is more likely to obtain good data, and so for this purpose we include a short description of the data collection process here. Using the Telescope Control System (TCS), an observer must first, after verifying that conditions are good (not too cloudy or humid), open the dome and enable dome tracking, so that the target star can be tracked as it moved across the sky. After the mirror covers are then opened, one is essentially ready to slew to a target star, using its RA and DEC positions. Once there, the observer can take a test image by trying out a sample exposure time. An ideal exposure lasts as long as possible without saturating any part of the image. If the brightness is suitable enough for .fit files, a guide star must then be selected, in order to track the target star with additional precision. The stars in the guider's field of view are outside of the telescope's main field of view, but close enough to track effectively. After the guider locks on to a suitable, bright guide star, the observer is ready to take a series of fit files that will last the duration of the transit.

4. Extracting the Data using Photutils

Over the course of the night, the telescope continued to track the targeted star and made regular observations. The measurements were saved to a local hard drive and transferred off-site via FTP. Though the data had been taken, it was not in a state ready for measurement. A telescope takes images of a field of view much wider than the target stars' radii, and so it was necessary to isolate individual stars in digital apertures with tools from the Photutils library. This was done twice per data-set: first with the DAOStarFinder method, to confirm exact initial coordinates of the target star and find nearby stars similar to it in brightness, and then later to measure the photon counts of the selected stars and save them in a more useful format. Because these observations were taken from a ground-based telescope, even a perfectly clear sky would have negatively impacted the quality of our data, as the mass of seemingly transparent air would change our data. Unfortunately, each night of observation also dealt with light to medium clouds that passed over time, significantly disrupting our measurements. In addition, Kitt Peak, though relatively isolated from large cities, still suffers from light pollution. To account for these, we used the Background2D method to iteratively compound estimates of median background brightness for each individual image, which we then subtracted from the image at large. For HAT-P-12, which drifted significantly across the field of view over the course of its observation, it was necessary to do these processes twice, first based on coordinates relevant at the beginning of the night, then with coordinates for the end of the night. We then plotted our target stars' counts alongside comparison stars' to better determine which nearby stars were best suited for detrending.

5. Selecting Comparison Stars

For each individual star it was necessary to manually select a number of nearby stars of comparable brightness for the sake of detrending. Theoretically, any atmospheric effects that affect one would similarly affect the other, so iteratively dividing a target's count by the sum of well-selected comparison stars' counts can effectively detrend atmospheric effects. We tried to select stars with similar behaviors in their curves, avoiding selecting stars that had deviant behaviors in their light curves since using stars with minimal irregularities would be the most useful for detrending. These irregularities may be due to hot pixels affected by cosmic rays or jitters in the telescope due to thermal shocks. For each star we initially selected four potential comparison stars and then compared their counts over time to see which were best for comparison.

TrES-3 was not near any star exceptionally close in brightness, but we found that all four of the potential comparison stars (Figure 1) followed similar enough patterns for use in detrending.

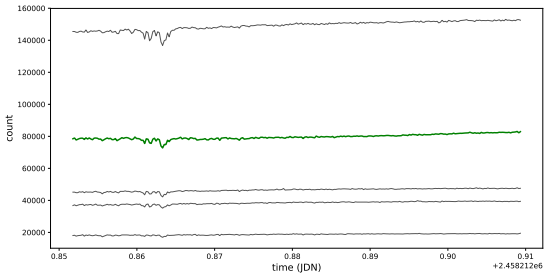

Fig. 1. TrES-3 alongside other background stars, before detrending.

HAT-P-12 was the brightest star within the field of view when measured, so we used the two next-brightest stars (Figure 2) to detrend it.

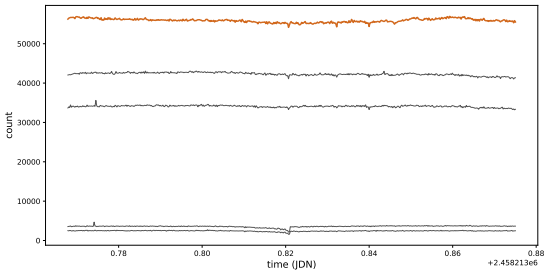

Fig. 2. HAT-P-12 alongside other background stars, before detrending.

HAT-P-26 was the second brightest star in its image, with only two stars of comparable brightness—one brighter, one dimmer. However, we saw that much less bright stars still followed the same trends and included two of them for detrending as well, allowing us to use all four of our selected comparison stars (Figure 3).

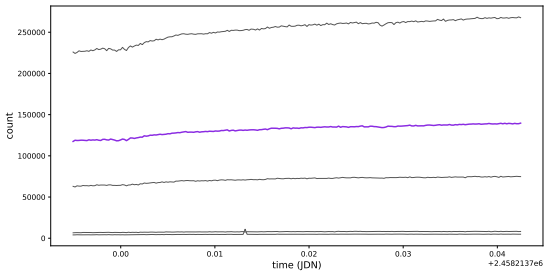

Fig. 3. HAT-P-26 alongside other background stars, before detrending.

HATS-18 was the first transit we observed in this project and proved to be difficult to work with. Detrending was complicated because there were no nearby stars that had a brightness value comparable to that of HATS-18. As seen in Figure 4, we were forced to settle for stars that were approximately only half as bright as the target star, limiting our ability to faithfully remove trends. An additional complication for HATS-18 in particular was that it had a low altitude on the sky (a factor that we considered more heavily for our later target stars). Once again, observing a low altitude star means observing a target obstructed by high levels of air mass. This, along with heavy clouds in the sky during observing time, plagues our analysis of HATS-18 from detrending to depth measurement.

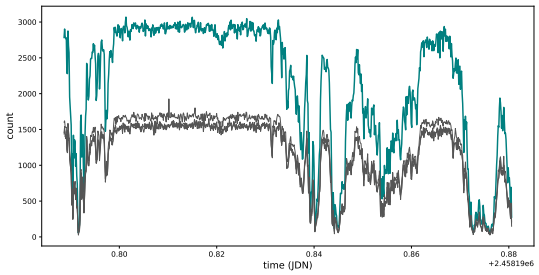

Fig. 4. HATS-18 alongside other background stars, before detrending.

XO-2 was almost identical in brightness to a nearby star, so even though we had found four potential comparison stars (Figure 5), we found the detrending worked best when we used only the one comparison star.

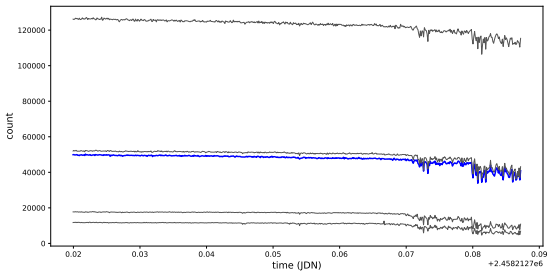

Fig. 5. XO-2 alongside other background stars, before detrending.

6. Detrending the Light Curves

After these procedures, transits were still indiscernible in plotted data. We found it necessary to perform additional detrending based on stars near and similar in brightness to each target. First we normalized the data for each star by dividing it by its own average counts. We then simply divided the normalized counts of our target stars by the normalized counts of their partner stars. As long as partner stars were appropriately chosen and the observations were performed adequately, this led to visible light curves in the detrended target stars' data.

Unfortunately, some target stars had few nearby stars similar in brightness, and others were subject to strange perturbations which made detrending difficult. Some of the culprits for these disruptions are thick clouds passing during the transit, errors in the guiding system of the telescope, and faulty pixels on the telescope's detector that happened to be near the targets. Luckily, two of our observations yielded a clear light curve as expected. TrES-3, in particular, showed a standout light curve, confirming our foreknowledge of the exoplanet TrES-3 b (see Figure 6. HAT-P-12 initially showed no clear pattern until the data was extracted from two sets of coordinates, after which a distinct light curve became visible (Figure 7. Two observations intended to be of half-transits, failed to actually measure all the way to the midpoint, which made their depths less useful, but also affected detrending, since our method works better with more data points. These stars' (XO-2, Figure 10 and HAT-P-26, Figure 8) data are included for reference, but any depth was treated as a minimum measurement. Therefore, the predicted planetary radius for said stars is only a minimum possible value. While HATS-18 was observed for the duration of a full transit, it is clear from Figure 9 that no clear transit can be detected, even after being treated with a moving median (see Figure 14, probably due to one or more of the reasons mentioned above.

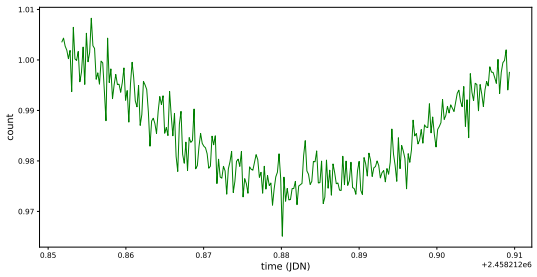

Fig. 6. TrES-3 after dividing by fluxes from other stars.

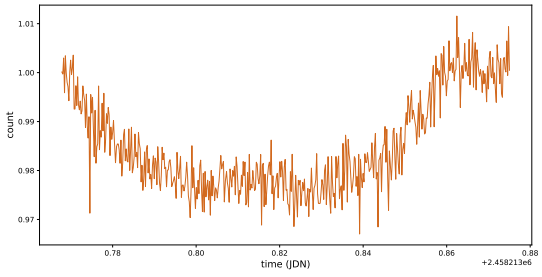

Fig. 7. HAT-P-12 after dividing by fluxes from other stars.

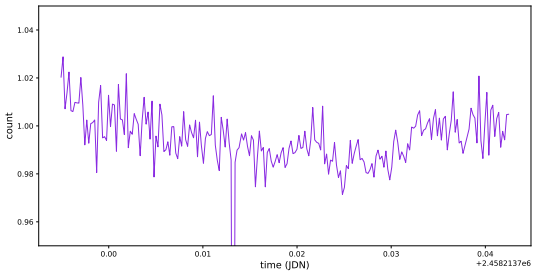

Fig. 8. HAT-P-26 after dividing by fluxes from other stars.

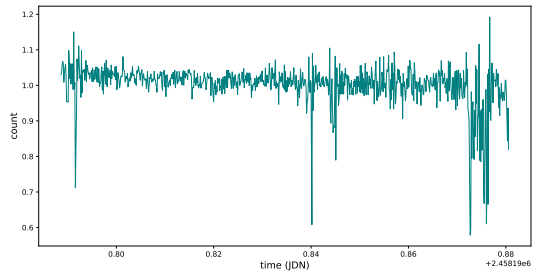

Fig. 9. HATS-18 after dividing by fluxes from other stars.

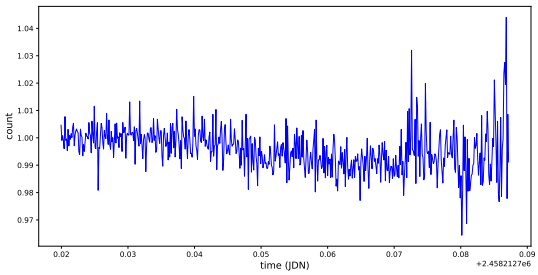

Fig. 10. XO-2 after dividing by fluxes from other stars.

7. Results

To clarify light curves, we ran moving median reductions over noisy, detrended data. The window size for these moving median implementations were adjusted individually for each transit, but remained approximately 5% of the number of data points, so as to only eradicate noise instead of large trends taken care of by our previous detrending method. Moving medians not only made depth calculations easier for the well-behaved light curves, but also helped solidify which observations actually showed measurable transits. As predicted early on, HATS-18 proved to be problematic because of its combination of a cloudy sky and a high air mass, even though it was observed for a full transit duration. One can observe the difference a moving median makes by comparing Figures 9 and 14. With a moving median, noise and some short-term drastic spikes are removed. However, we can see more clearly that our HATS-18 observation would not yield a useful depth measurement, because of the very prominent spike towards the end. This disruption affected our depth calculation and resulted in a obviously incorrect negative depth value. The moving median also revealed how important it was, at least for the procedures we used, to reach the mid-transit time in our observations. As seen in Figures 13 and 15, the light curve quickly rises towards the end of the observation time, again interfering with our depth calculations. Luckily, the post-moving median versions of TrES-3 and HAT-P-12 yield classically beautiful and measurable transits (Figures 11 and 12, respectively).

7.1. TrES-3

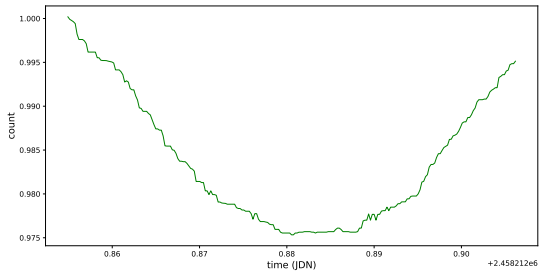

Fig. 11. TrES-3b after moving median. Beautiful transit. Measured depth of 0.0246673139856.

7.2. HAT-P-12

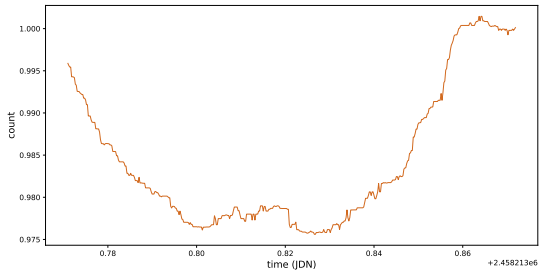

Fig. 12. HAT-P-12b after moving median. Clear transit. Measured depth of 0.0243943110206.

7.3. HAT-P-26

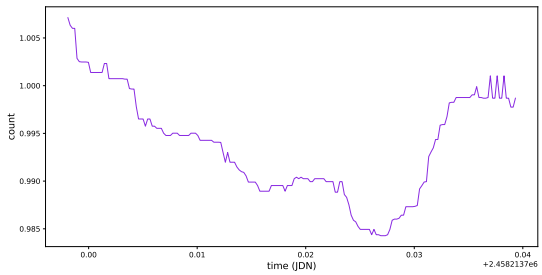

Fig. 13. Incomplete first half of HAT-P-26 b transit after moving median. The photon count declines as expected to for this transit, but then unexpectedly jumps up near the end. Collection of data was cut short before the midpoint, making true depth impossible to measure and leading to detrending problems that could explain the plateau near the end.

7.4. HATS-18

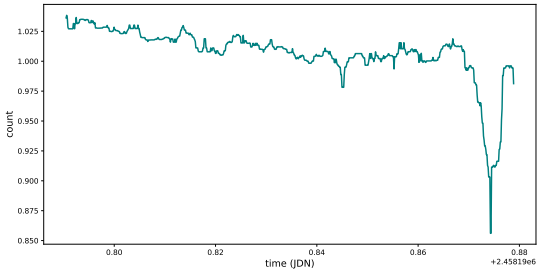

Fig. 14. Full transit of HATS-18b. Shows no clear transit.

7.5. XO-2

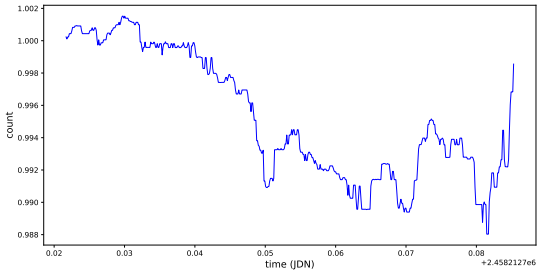

Fig. 15. XO-2 b after moving median. This observation was meant to be the first half of a transit, but was cut short. It clearly declines, but in an unexpected and inconsistent manner.

8. Analyzing the Data

Determining a transiting planet's density can be very useful in order to learn more about the transiting planet's physical structure. This can help us determine what exoplanet class the transiting world might belong to, informing us if the planet is more like a gas giant or a rocky planet.

Once we detect the transit of an exoplanet, we can use the light curve to gather physical information about it. A major advantage of the transit method is that the planetary radius can be calculated from the light curve. The amount of light the transiting planet blocks depends on its size, and so using the measurement of the transit depth and the size of the star, which is generally determined from ground-based observations of the star's spectral type, the size of the planet can be calculated. The expression relating the radii and the transit depth can be expressed as

$$R_p = R_* \sqrt{\delta}$$

where R_p is the planetary radius, R_* is the stellar radius, and δ is the transit depth.

The radius of TrES-3b using this method was found to be $1.268^{+0.023}_{-0.034} R_J$ with $\delta = 0.0247$, having a percentage difference of approximately 5 percent compared to the value we found in another study of $1.336^{+0.031}_{-0.036} R_J$. We also were able to calculate a radius of $1.066^{+0.026}_{-0.018} R_J$ with $\delta = 0.0244$ for HAT-P-12b, approximately an 11 percent error in comparison to the value of $0.959^{+0.029}_{-0.021} R_J$ we found in literature.

Given the orbital period, inclination angle of the orbital plane, and the stellar mass, one could use these along with precise radial velocity measurements to solve for the mass of the planet. However, this would require a high-resolution spectrograph, which we did not have at our disposal. As an alternative, we found a value for planetary mass by looking at other studies. With this known and planetary radius, we can solve for average density.

The mean density of TrES-3b, which has a mass of $1.910^{+0.075}_{-0.080} M_J$, we found to be $1.239^{+0.157}_{-0.114} gcm^{-3}$. This result along with TrES-3b's short orbital period of around 1.3 days indicates that it is a hot Jupiter. The mean density of HAT-P-12b, which has a mass of $0.211 \pm 0.012 M_J$, we found to be $0.23^{+0.026}_{-0.028} gcm^{-3}$, which is comparable to the value of $0.295 \pm 0.025 gcm^{-3}$ found in another study. This very small result indicates HAT-P-12b is a gaseous sub-Saturn planet. Both of these classifications are in agreement with what we found in literature.

Unfortunately, as previously mentioned, TrES-3b and HAT-P-12b were the only targets that we were able to collect transit depths for; the other targets' data was either incomplete or flawed. As seen in Figures 13 and 15, the transits were cut short which prevented us from getting the transit depths of the light curves, while in Figure 14 the transit was marred with a high air mass and occasional clouds which confounded the data beyond the reach of our detrending methods.

9. Other Properties of Planets

The planets that we attempted to detect have already been discovered and studied, TrES-3 in particular. Sozzetti et al. 2009, for example, was able to acquire new new radial velocity and photometric observations of TrES-3 with which they refined both the light-curve solution and the spectroscopic orbit of TrES-3 from its discovery paper.

An abundance analysis was carried out using the Keck/HIRES template spectra of TrES-3, from which the stellar atmosphere parameters of [Fe / H], T_{eff}, and $log(g)$ were determined. This analysis yields $T_{eff} = 5650 \pm 75K$, and $log(g) = 4.4 \pm 0.1$. Also, TrES-3 has a mass of $1.910 \pm 0.075 M_J$, and a radius of $1.336 \pm 0.031 M_J$. Thus, TrES-3 can be categorized as a hot Jupiter. Compared to Earth's effective temperature of 252 K, TrES-3 is much hotter. Compared to Earth's $log(g)$ of 2.992, TrES-3 has a much greater surface gravity.

Hartman et al. 2009 found that HAT-P-12b has a mass of $0.211 \pm 0.012 M_J$ and radius of $0.959 \pm 0.029 R_J$, and proposes that it is a H/He-dominated planet. In fact, HAT-P-12b is the least massive H/He-dominated gas giant planet found to date.

Penev et al. 2016 found that HATS-18b has a mass of $1.980 \pm 0.077 M_J$ and a radius of $1.337 \pm 0.012 R_J$. Moreover, the planet has a 0.8378 day orbit. As a result of the planet's high mass and close orbit, Penev et al. suggest that there exists strong tidal coupling between the planetary orbit and the star. The host star HATS-18 shows evidence of significant tidal spin up.

Burke et al. 2007 found that XO-2, a hot Jupiter, has a mass of $0.57 \pm 0.06 M_J$ and a radius of $0.98 \pm 0.01 R_J$.

Hartman et al. 2011 found that HAT-P-26b has a mass of $0.059 \pm 0.007 M_J$ and a radius of $0.565 \pm 0.072 R_J$, making it a low density Neptune-mass planet.

10. Conclusion

These results are an excellent example of the ability of smaller telescopes, like MDM's McGraw-Hill, to conduct time series photometry for exoplanet detection.

This project was as much a learning experience as it was a scientific exercise. We were able to engage with the entire process from data collection and telescope operation to analyzing and presenting the data collected. We each got the opportunity to familiarize ourselves with in-person and remote operation of large professional telescopes. We developed our intuition for the effects heavy clouds and high air mass have on specific observations. In the future, we will know to take the time to capture extra photometry at each end of our observations. In general, this has been an excellent opportunity for us as aspiring astronomers to hone our skills performing observation, data analysis, academic reading, and scientific writing.

11. Acknowledgements

Thank you David, Jose, and the entire state of Arizona.

References

Burke, C. J., McCullough, P. R., Valenti, J. A., et al. 2007, ApJ, 671, 2115
Hartman, J. D., Bakos, G. Á., Kipping, D. M., et al. 2011, ApJ, 728, 138
Hartman, J. D., Bakos, G. Á., Torres, G., et al. 2009, ApJ, 706, 785
Penev, K., Hartman, J. D., Bakos, G. Á., et al. 2016, AJ, 152, 127
Sozzetti, A., Torres, G., Charbonneau, D., et al. 2009, ApJ, 691, 1145